MODELING THE SOUTH POLE-AITKEN BASIN SUBSURFACE. W. M. Vaughan[1] and J. W. Head[1].
[1]Department of Geological Sciences, Brown University, Providence, RI 02912, USA, Will_Vaughan@brown.edu.

Introduction: Recent multispectral surveys [1-13] indicate that the South Pole-Aitken basin (SPA) subsurface is lithologically diverse. Mare basalts and norites are exposed at the surface [1,3,10,12]; crater central peaks superposing SPA expose low-Ca pyroxene-rich lithologies, possibly pyroxenite, from depths of ~10–20 km [2,4,5-9,11-13]; the largest craters and basins superposing SPA expose olivine-bearing lithologies from up to ~40 km depth [8,13]. Thus, a vertical span of ~40 km, which is now thought to be the average thickness of the anorthositic lunar crust [14], unusually contains typical lower crustal and upper mantle lithologies. How should the remarkable (and clearly atypical [8,9,12]) lithological diversity of the SPA subsurface be interpreted?

A natural interpretation is that the SPA-forming impact excavated the anorthositic upper crust and that noritic and ultramafic lithologies in SPA represent exposures of the lower crust and upper mantle. Yet this interpretation seems to be at odds with what is known about the basin-forming process and the nature of the lunar upper mantle. First, since basins less than half the diameter of SPA excavate well into the lunar crust [15] (and possibly into the upper mantle [8]), scaling relationships [15] indicate that the SPA-forming impact should have excavated a cavity hundreds of kilometers deep, well into the upper mantle; thus, no noritic material should remain in the basin interior and ultramafic lithologies should be exposed at the surface. (SPA is elliptical [16], apparently formed by an oblique impact; it has been suggested [17] that an oblique SPA-forming impact might excavate a very shallow cavity; regardless, as will be discussed next, ultramafic lithologies in SPA do not resemble upper mantle lithologies.) Second, the ultramafic lithologies occurring in the SPA subsurface are mainly olivine-free pyroxenite [7]. Yet the lunar upper mantle ought to contain olivine in addition to pyroxene, as suggested by lines of evidence as diverse as thermodynamic inversions of seismic data [18] and exposures of olivine in basin ejecta [8]. It therefore seems that the SPA subsurface is not simply a section of the lower crust and upper mantle.

A more recent (and more promising) interpretation is that noritic and ultramafic lithologies in the SPA subsurface were formed by the differentiation of a massive impact melt sheet generated by the SPA-forming impact [19-22]. Large basin-forming impacts melt nearly as much material as they excavate [23]. Scaling laws predict the largest lunar basin-forming impacts produce ~10^7 km^3 of shock melt [23-24].

Much of this impact melt is retained inside the final crater [23], forming an enormous lens of impact melt (an impact melt sea [21]). Study of impact melt bodies in large terrestrial craters, such as Sudbury [20], suggest that impact melt undergoes extensive igneous differentiation by crystal settling to form enormous, locally homogenous igneous strata. Qualitatively, igneous differentiation of an impact melt sea generated by the SPA-forming impact should give rise to an olivine-rich cumulate (dunite) overlain by a pyroxene-rich cumulate (pyroxenite) which is in turn overlain by plagioclase-bearing lithologies, exactly as is the case in SPA (an insightful observation first made by Morrison in 1998 [19]). The idea that the SPA subsurface is a differentiated mixture of crust and mantle explains several apparent paradoxes—mantle olivine, mostly absent from the SPA subsurface, is locked in deep dunite; surficial norite is not lower crust, but a late-stage plagioclase-rich cumulate.

The impact melt differentiation model for the SPA subsurface [19] has not yet been rendered quantitative: it does not predict, *e.g.*, the thickness and average Mg number of a cumulate layer. In this abstract, we build on our recent work, which quantitatively investigates lunar impact melt differentiation [21], to produce a model of the cumulate layers comprising the SPA subsurface. We then compare the predictions of this model to constraints on the SPA subsurface [1-13].

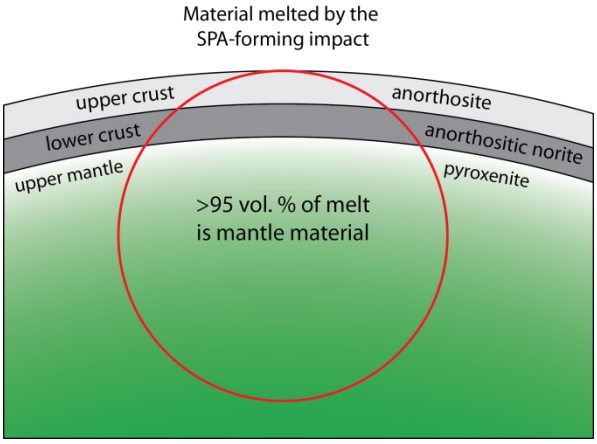

Figure 1. Bulk composition of SPA impact melt (melt cavity superposed on lunar crust and upper mantle). Crustal thickness is exaggerated by a factor of 2.

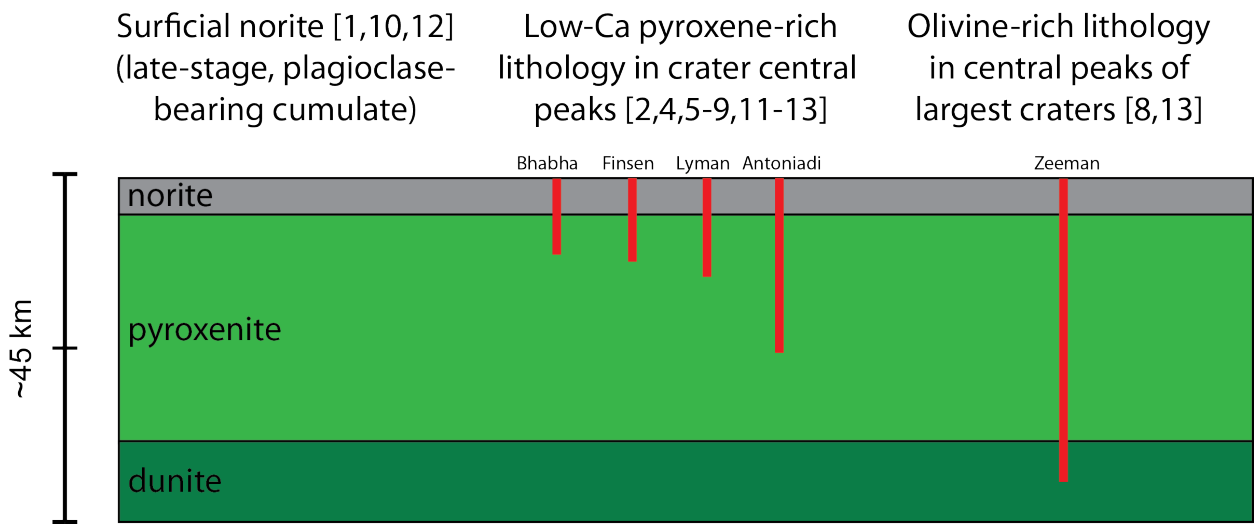

Figure 2. The modeled cumulate stratigraphy of the SPA subsurface agrees closely with constraints from [1-13].

Modeling the SPA subsurface:

Volume and geometry of the SPA melt cavity. We take the SPA transient cavity diameter to be 2099 km [15]. Using the impact melt volume scaling relationship derived by [24], we estimate that the SPA-forming impact produced ~6.8 × 10^7 km^3 of impact melt (in reasonable agreement with [22]). A spherical melt cavity containing ~6.8 × 10^7 km^3 of melt is ~500 km in diameter; the SPA-forming impact thus likely melted well into the lunar mantle. Such a spherical melt cavity is shown superposed on the pre-existing structure of the lunar crust [14] and mantle in Figure 1 above. Notice >95 vol. % of the melt is mantle material.

Bulk compostion of SPA impact melt. We calculate the bulk composition of SPA impact melt as a mixture of crust and mantle compositions in proportions suggested by Figure 1, assuming that the crust and mantle are composed entirely of plagioclase (anorthite), pyroxene (enstatite), and olivine (forsterite). See [21] for additional details. The bulk composition of the impact melt is similar to the composition of the upper mantle, with pyroxene and olivine in upper mantle proportions (probably ~3:1 [18]), and minor plagioclase (<5 vol. %) from crustal melt.

Geometry and thickness of the SPA melt sea. ~25 vol. % of the total melt produced was likely excavated in forming the SPA transient cavity [23], leaving ~5 × 10^7 km^3 of melt inside the transient cavity to form a melt sea. The final thickness of the melt sea is controlled by its areal extent. The inner ring of SPA can be approximated as an ellipse with semiminor and semimajor axes of 720 km and 970 km respectively [16]; a prismatic melt sea with this areal extent and this volume of melt is ~25 km thick. However, studies of the Orientale melt sea [21] indicate that most impact melt occurs inside a region with a diameter ~70% of that of the innermost basin ring; if this ratio holds for SPA, then the SPA melt sea may be ~45 km thick.

Cumulate stratigraphy of the SPA melt sea. We determine the equilibrium crystallization sequence of the bulk composition above using the An-Fo-Qz phase diagram (olivine → orthopyroxene → orthopyroxene + plagioclase). From a model of liquid density based on partial molar volumes, we determine that all solids (including plagioclase) are denser than coexisting liquids; the modeled crystallization sequence thus becomes the stratigraphic sequence. Finally, we use mass balance to find the proportions and thicknesses of each cumulate layer. Again, see [21] for additional details.

Results. The modeled cumulate stratigraphy agrees closely with constraints from [1-13] (Figure 2). In particular, we predict a homogenous pyroxenite cumulate ~30 km in thickness, which explains the otherwise puzzling central peak observations of [7]. A more detailed model which incorporates the effects of oblique impact and predicts the Mg number of cumulate layers is in preparation.

References: [1] Head J. W. et al. (1993) *JGR, 98*, 17149–17181. [2] Tompkins S. and C. M. Pieters (1999) *MAPS, 34*, 25–41. [3] Yingst R. A. and J. W. Head (1999) *JGR, 104*. [4] Pieters C. M. et al. (2001) *JGR, 106*, 28001–28002. [5] Matsunaga T. et al. (2008) *GRL, 35*. [6] Cahill J. T. S. et al. (2009) *JGR, 114*. [7] Nakamura R. et al. (2009) *GRL, 36*. [8] Yamamoto S. et al. (2010) *Nature Geosci.*, *3*, 533–536. [9] Klima R. L. et al. (2011) *JGR*, *116*. [10] Borst A. M. et al. (2012) *PSS, 68*, 76–85. [11] Moriarty D. P. et al. (2012) *LPS, 43*. [12] Nakamura R. et al. (2012) *Nature Geosci., 5*, 775–778. [13] Yamamoto S. et al. (2012) *Icarus, 218*, 331–344. [14] Wieczorek M. A. et al. (2012) *Science*. [15] Wieczorek M. A. and R. J. Phillips (1999) *Icarus, 139*, 246–259. [16] Garrick–Bethell I. and M. T. Zuber (2009) *Icarus, 204*, 399–408. [17] Schultz P. H. (1997) *LPS, 28*. [18] Khan A. (2006) *Geophys. J. Int., 168*, 243–258. [19] Morrison D. A. (1998) *LPS*, 29. [20] Grieve R. A. F. (1991) *JGR, 96*. [21] Vaughan W. M. et al. (2012) *Icarus*, in revision. [22] Potter R. K. et al. (2012) *Icarus, 220*, 730–743. [23] Cintala M. J. and R. A. F. Grieve (1998) *MAPS, 33*, 889–912. [24] Abramov O. et al. (2012) *Icarus, 218*, 905–916.